Matching of electronic wavefunctions and envelope functions at GaAs/AlAs interfaces

1992 J. Phys.: Condens. Matter 4 2587

(http://iopscience.iop.org/0953-8984/4/10/021)

J. Phys.: Condens. Matter 4 (1992) 2587–2608. Printed in the UK

Matching of electronic wavefunctions and envelope functions at GaAs/AlAs interfaces

J P Cuypers and W van Haeringen

Eindhoven University of Technology, Department of Physics, PO Box 513, 5600 MB Eindhoven, The Netherlands

Received 21 June 1991, in final form 28 October 1991

Abstract. A method to calculate electronic wavefunctions and energies in AlGaAs heterostructures is developed and applied to some typical configurations. The method is based on the use of empirical pseudopotentials and the applicability of the flat-band approximation. Coupling of Γ- and X-like conduction-band electrons is explicitly dealt with. Emphasis is put on the precise matching of wavefunctions at interfaces as well as on the connection rules for the related envelope functions. Among other things, we do not find evidence for boundary conditions for derivatives of envelope functions involving effective mass ratios.

1. Introduction

There is great interest in theoretical calculations on electronic states in heterostructures. The most rigorous approach is to use self-consistent supercell calculations (Van de Walle and Martin 1987, Baldereschi *et al* 1988, Picket *et al* 1978). These calculations, however, are restricted to superlattices with relatively small width layers only. Moreover, the emphasis in such kind of calculations is on ground state properties. If we are interested in conduction-band state wavefunctions and energies, say, it is more appropriate to use less rigorous methods. One of the objectives of this paper is to perform calculations of electronic wavefunctions in the particular class of heterostructures composed of $Al_xGa_{1-x}As$ layers. In doing so, we base ourselves on (complex) bandstructures and wavefunctions (Heine 1963) for the respective sublayer materials, to be obtained within the empirical pseudopotential method (EPM) (Cohen and Bergstresser 1966, Baldereschi *et al* 1977). Matching at interfaces of wavefunctions is achieved by demanding continuity of a sufficient number of z-dependent (z denotes the direction perpendicular to the interface) two-dimensional (2D) Fourier coefficients of the entire wavefunction as well as continuity of their derivatives with respect to z. Our approach, which shows both similarities and differences with the approach of e.g. Marsh and Inkson (1986), Ko and Inkson (1988), Edwards and Inkson (1990) and Brand and Hughes (1987), will be illustrated for the cases of one and two interfaces, but can easily be extended to more interfaces. A second objective is to actually construct, from the above EPM obtained wavefunctions in the heterostructure, the related envelope functions, according to the Lüttinger–Kohn definition (Lüttinger and Kohn 1955). This construction of the actual envelope functions enables us to determine what kind of boundary conditions these functions apparently have to fulfill. These

0953-8984/92/102587+22$04.50

can then subsequently be compared with connection prescriptions as used in the literature, (e.g. Altarelli 1983, Ando *et al* 1989, Bastard 1981, Burt 1989, Eppenga *et al* 1985, Hurkx and van Haeringen 1985, Pötz and Ferry 1987, Schuurmans and 't Hooft 1985, Smith and Mailhiot 1986).

The paper is organized as follows. Section 2 deals with the empirical pseudopotential method for calculating electronic states in heterostructures, in the framework of the flat band approximation (FBA) which is introduced in section 2.1. Complex bandstructures are discussed in section 2.2, while boundary conditions are formulated in section 2.3. The method of constructing envelope functions is described in section 3. Section 4 is devoted to the scattering of electrons at a single GaAs/AlAs interface. Scattering coefficients belonging to various channels are explicitly calculated as a function of energy. Section 4.2 is more specifically devoted to the connection rules for envelope functions which can be deduced from this treatment of the electron scattering problem. Section 5 deals with the tunnelling of electrons through a GaAs/$Al_xGa_{1-x}As$/GaAs barrier structure, and compares obtained EPM results with results obtained from models in which envelope functions are used which are assumed to fulfil simplified connection rules. It appears, among other things, that for energies above the X-minimum in the conduction band of AlAs, the Γ-band electrons tunnel resonantly through the X-valley quantum well in AlAs. Both the results of our method to obtain the true electronic wavefunctions as well as our findings concerning the connection rules for envelope functions are summarized in section 6. An important result is that no evidence is found for a connection rule for derivatives of envelope functions involving effective mass ratios.

2. Empirical pseudopotential method for lattice matched heterostructures

In this section we will give an outline of a method to obtain electronic wavefunctions in a lattice matched heterostructure. The method is based on the use of empirical pseudopotentials and is highly similar to the one used by Brand and Hughes (1987) and by Marsh and Inkson (1986), although there are notable differences in numerical implementation. The section will be subdivided into three parts, the first of which will be concerned with the introduction of the flat-band approximation. The second will be devoted to the calculation of complex bandstructures and the corresponding eigenfunctions. The third section deals with the boundary conditions, and their role in determining the scattering characteristics of electrons at a single interface as well as at barriers (wells) consisting of two or more interfaces.

2.1. Flat-band approximation

Although the flat-band approximation (FBA) is a very common *ansatz* in calculations of electronic states in heterostructures, we consider it necessary to state precisely what we mean by it. As is well known from self-consistent supercell calculations (Van de Walle and Martin 1987, Pickett *et al* 1978, Baldereschi *et al* 1988), the full self-consistent potential in a sublayer of a lattice matched heterostructure is identical to the bulk-potential of the corresponding material, except at distances in the direct neighbourhood of the interface. In figure 1 we have plotted the most important 2D Fourier coefficients of the difference between the self-consistent heterostructure potential and the self-consistent bulk-potential of the involved sublayer material for a

GaAs/AlAs supercell along the [001] direction. These results were obtained by *ab initio* self-consistent supercell calculations, using norm-conserving pseudopotentials and the LDA approximation, performed by Van de Walle and Martin (1987). As can be seen in figure 1, the difference potentials are only appreciably non-zero within one monolayer thickness from the interface. We define the FBA by approximating the potential in a heterostructure layer by means of the potential of the corresponding perfect bulk-material, and by using experimentally or theoretically obtained band offset parameters in order to position the energy bands of neighbouring sublayers. According to figure 1 this approximation neglects the effects of small regions near the interfaces. Note, however, that the strength of the neglected difference potential near the interface may be appreciable and e.g. comparable to the valence band offset. Whether this may invalidate FBA obtained results has to be the subject of further study.

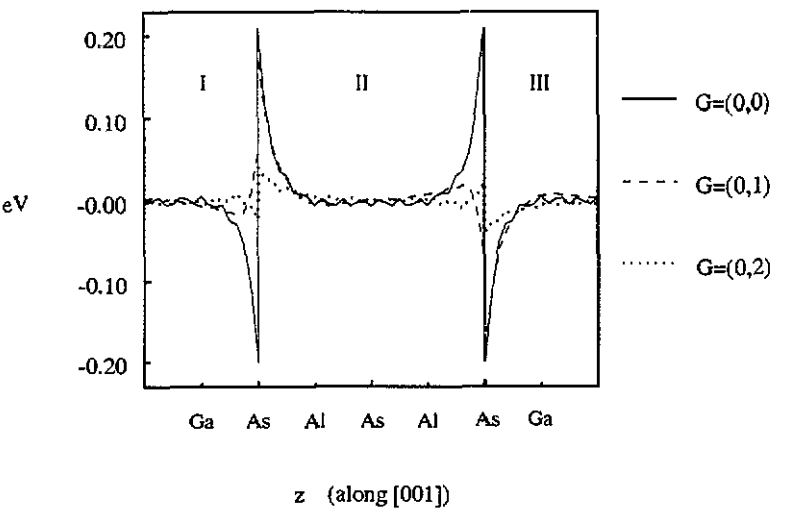

Figure 1. Difference potential Fourier coefficient $U_G(z)$ along [001] between the total self-consistent potential of a GaAs/AlAs-based superlattice and the corresponding bulk potential (GaAs in regions I and III, AlAs in region II) obtained by self-consistent *ab initio* pseudopotential calculations (Van de Walle and Martin 1987) for $G = (0,0)$ (solid curve), $G = (0,1)$ (dashed curve), and $G = (0,2)$ (dotted curve), where $G = (0,1)$ are basis vectors of the two-dimensional reciprocal lattice. The location of the interfaces is chosen at the As-planes such that the strength of the $U_G(z)$-potentials is as small as possible. The $U_G(z)$-potentials are zero (except for small fluctuations due to numerical noise) except within one monolayer thickness of the interfaces. The amplitudes are however comparable with e.g. the valence band offset $\Delta E_v \approx 0.4$ eV.

We propose to choose the position z_0 of the interface in the FBA scheme by means of the criterion $\int \Delta V_{G=0}(z - z_0)dz = 0$, where ΔV is the above mentioned difference potential. We observe from figure 1 that z_0 almost precisely coincides with the As-plane for the case of a GaAs/AlAs [001] interface.

2.2. Calculation of complex bandstructures

In FBA we now use the following procedure. For each material layer j the Schrödinger equation is solved for the *infinite* perfect bulk-crystal of material j at given energy

E and parallel wavevector $q_\parallel$. The general solution in each layer is then a linear combination of all possible solutions at that energy and $q_\parallel$. Boundary conditions at all interfaces and at $z = \pm\infty$ will then fix the solution valid for the entire heterostructure.

We start with the one-electron Schrödinger equation for a bulk-crystal of material j ($\hbar = 1, m = \frac{1}{2}$)

$$[-\nabla^2 + V^j(\boldsymbol{r}) + U_0^j]\psi^j(\boldsymbol{r}) = E\psi^j(\boldsymbol{r}) \tag{1}$$

where $V^j(\boldsymbol{r})$ is a local empirical pseudopotential, reproducing the bandstructure of material j to reasonable accuracy. Note that we added an unknown constant U_0^j in equation (1) for each material j. These constants have to account for the valence band offset parameters between the respective material layers. We neglect spin-orbit interaction for the sake of simplicity, but this can easily be added if necessary. Since $V^j(\boldsymbol{r})$ is periodic in three dimensions, solutions of equation (1), at given E and $q_\parallel$, can be written as the generalized Bloch functions (Mott and Jones 1936)

$$\psi^j(\boldsymbol{r}) = \mathrm{e}^{\mathrm{i}\boldsymbol{k}^j\cdot\boldsymbol{r}}u^j(\boldsymbol{r}) = \mathrm{e}^{\mathrm{i}\boldsymbol{q}_\parallel\cdot\boldsymbol{\rho}}\mathrm{e}^{\mathrm{i}k_z^j z}u^j(\boldsymbol{r}) \tag{2}$$

where k_z^j is either real or complex. Expanding the $u^j(\boldsymbol{r})$-functions in plane waves $\mathrm{e}^{\mathrm{i}\boldsymbol{K}\cdot\boldsymbol{r}}$, $\boldsymbol{K}$ being reciprocal lattice vectors, we obtain a matrix equation for k_z^j. If N plane waves are used there are $2N$ solutions (which will be labelled with index s). However, only the in-zone solutions should be retained, the number of which equals $2M$, where M is the number of projected reciprocal lattice vectors $\boldsymbol{G}$, with $\boldsymbol{K} = \boldsymbol{G} + G_z\boldsymbol{e}_z$ (the proof is given in appendix A). The general wavefunction solution in each layer j can now be written as a linear combination of all possible Bloch-type solutions with different $k_z^{j,s}$

$$\psi^j(\boldsymbol{r}) = \sum_s^{2M} \alpha^{j,s}\psi^{j,s}(\boldsymbol{r}) \tag{3}$$

where $\psi^{j,s}(\boldsymbol{r})$ is given by equation (2). The coefficients $\alpha^{j,s}$ have to be fixed by the boundary conditions.

2.3. Boundary conditions

We will now formulate the boundary conditions at an interface which will be expressed in terms of an **S**-matrix, describing the scattering of an electron at a single interface. In addition the boundary conditions at the two interfaces of a single barrier or QW structure will be formulated in such a way, that a numerical stable solution can easily be obtained.

Using translational symmetry in the x-, y-directions we write

$$\psi^j(\boldsymbol{r}) = \sum_{\boldsymbol{G}} \mathrm{e}^{\mathrm{i}(\boldsymbol{q}_\parallel+\boldsymbol{G})\cdot\boldsymbol{\rho}}v_{\boldsymbol{G}}^j(z) \tag{4}$$

where $\boldsymbol{\rho} = (x, y)$ and according to (3) and (2)

$$v_{\boldsymbol{G}}^j(z) = \sum_s^{2M} \alpha^{j,s}v_{\boldsymbol{G}}^{j,s}(z) \tag{5}$$

with

$$v_G^{j,s}(z) = \mathrm{e}^{\mathrm{i}k_z^{j,s}z} u_G^{j,s}(z) \tag{6}$$

the $u_G^{j,s}(z)$-functions being the 2D Fourier coefficients of the $u^{j,s}(\boldsymbol{r})$-functions in equation (2),

$$u^{j,s}(\boldsymbol{r}) = \sum_{\boldsymbol{G}} \mathrm{e}^{\mathrm{i}\boldsymbol{G}\cdot\boldsymbol{\rho}} u_G^{j,s}(z)\,. \tag{7}$$

The boundary conditions follow from demanding $v_G^j(z)$ and its first derivative to be continuous at the interface (located at z_0) for all $\boldsymbol{G}$

$$\sum_s^{2M} \alpha^{j,s} v_G^{j,s}(z_0) = \sum_s^{2M} \alpha^{j+1,s} v_G^{j+1,s}(z_0) \tag{8}$$

and

$$\sum_s^{2M} \alpha^{j,s} \left.\frac{\partial v_G^{j,s}(z)}{\partial z}\right|_{z_0} = \sum_s^{2M} \alpha^{j+1,s} \left.\frac{\partial v_G^{j+1,s}(z)}{\partial z}\right|_{z_0}. \tag{9}$$

Equations (8) and (9) constitute $2M$ equations (M $\boldsymbol{G}$-vectors) which, together with $2M$ conditions at $z = \pm\infty$, fix all constants $\alpha^{j,s}$ in their respective layers. It is convenient to write (8) and (9) in matrix notation

$$\mathbf{D}^j(z_0)\boldsymbol{\alpha}^j = \mathbf{D}^{j+1}(z_0)\boldsymbol{\alpha}^{j+1}\,. \tag{10}$$

The $\mathbf{D}^j(z_0)$-matrices are $2M \times 2M$ matrices, the elements of which follow in an obvious way from equations (8) and (9). In order to obtain an **S**-matrix description we first rewrite (10) in the form

$$\begin{pmatrix} \mathbf{D}^{j,\rightarrow}(z_0) & \mathbf{D}^{j,\leftarrow}(z_0) \end{pmatrix} \begin{pmatrix} \boldsymbol{\alpha}^{j,\rightarrow} \\ \boldsymbol{\alpha}^{j,\leftarrow} \end{pmatrix} = \begin{pmatrix} \mathbf{D}^{j+1,\rightarrow}(z_0) & \mathbf{D}^{j+1,\leftarrow}(z_0) \end{pmatrix} \begin{pmatrix} \boldsymbol{\alpha}^{j+1,\rightarrow} \\ \boldsymbol{\alpha}^{j+1,\leftarrow} \end{pmatrix} \tag{11}$$

where the right (left) arrow stands for Bloch/evanescent waves which travel/decay to the right (left). The $\mathbf{D}^{j,\rightarrow}(z_0)$ and $\mathbf{D}^{j,\leftarrow}(z_0)$ are $2M \times M$ matrices. We subsequently rewrite (11) as

$$\begin{pmatrix} -\mathbf{D}^{j+1,\rightarrow}(z_0) & \mathbf{D}^{j,\leftarrow}(z_0) \end{pmatrix} \begin{pmatrix} \boldsymbol{\alpha}^{j+1,\rightarrow} \\ \boldsymbol{\alpha}^{j,\leftarrow} \end{pmatrix} = \begin{pmatrix} -\mathbf{D}^{j,\rightarrow}(z_0) & \mathbf{D}^{j+1,\leftarrow}(z_0) \end{pmatrix} \begin{pmatrix} \boldsymbol{\alpha}^{j,\rightarrow} \\ \boldsymbol{\alpha}^{j+1,\leftarrow} \end{pmatrix} \tag{12}$$

where all outgoing channels (transmitted and reflected) are placed at the LHS, and all incident channels at the RHS, so

$$\mathbf{D}^{\mathrm{out}}(z_0)\boldsymbol{\alpha}^{\mathrm{out}} = \mathbf{D}^{\mathrm{in}}(z_0)\boldsymbol{\alpha}^{\mathrm{in}}\,. \tag{13}$$

The **S**-matrix is now defined as

$$\boldsymbol{\alpha}^{\mathrm{out}} = \mathbf{S}\boldsymbol{\alpha}^{\mathrm{in}} \tag{14}$$

with

$$\mathbf{S} = (\mathbf{D}^{\text{out}})^{-1}\mathbf{D}^{\text{in}}. \tag{15}$$

We may choose one incoming channel (for instance an incoming electron) corresponding to an $\boldsymbol{\alpha}^{\text{in}}$ vector with zero components except for one $\alpha^{j,\rightarrow}$-coefficient (corresponding to the incoming electron) which is equal to 1. The outgoing channels are then given by a row of the **S**-matrix.

In dealing with the situation with two interfaces, separated by a distance W, we have to take special care to avoid numerical problems. As has already been reported by Brand and Hughes (1987), and Ko and Inkson (1988), evanescent waves, corresponding to complex k_z-values with large imaginary parts may, even for relatively small barriers, lead to numerical problems. This problem is solved by applying either a numerical truncation scheme (Brand and Hughes) or a scattering matrix approach (Ko and Inkson). In this paper we present an alternative approach, also based on scattering matrices.

The tunnelling of an electron through a barrier is in fact the subsequent scattering of an electron at two interfaces. We therefore have to deal with incoming and outgoing channels at each interface again. In order to avoid manipulation with large numbers, we consider the waves in the barrier which are travelling/decaying to the right as outgoing from the *first* interface (coming from the left), and waves travelling/decaying to the left as outgoing from the *second* interface. Their amplitudes at the other interface are then either of similar magnitude (travelling waves) or are smaller (decaying waves). If the two interface positions are at z_0 and $z_0 + W$, then we suppress the occurrence of large numbers by alternately choosing the zero of the z-axis at z_0 or $z_0 + W$, which leads to the following boundary conditions at the first interface

$$\mathbf{D}^{j,\rightarrow}(0)\boldsymbol{\alpha}^{j,\rightarrow} + \mathbf{D}^{j,\leftarrow}(0)\boldsymbol{\alpha}^{j,\leftarrow} = \mathbf{D}^{j+1,\rightarrow}(0)\boldsymbol{\alpha}^{j+1,\rightarrow} + \mathbf{D}^{j+1,\leftarrow}(-W)\boldsymbol{\alpha}^{j+1,\leftarrow} \tag{16}$$

and at the second interface

$$\mathbf{D}^{j+1,\rightarrow}(W)\boldsymbol{\alpha}^{j+1,\rightarrow} + \mathbf{D}^{j+1,\leftarrow}(0)\boldsymbol{\alpha}^{j+1,\leftarrow} = \mathbf{D}^{j+2,\rightarrow}(0)\boldsymbol{\alpha}^{j+2,\rightarrow} + \mathbf{D}^{j+2,\leftarrow}(0)\boldsymbol{\alpha}^{j+2,\leftarrow}. \tag{17}$$

We rewrite this as

$$\begin{pmatrix} \mathbf{D}^{j,\rightarrow}(0) & -\mathbf{D}^{j+1,\rightarrow}(0) & -\mathbf{D}^{j+1,\leftarrow}(-W) & 0 \\ 0 & -\mathbf{D}^{j+1,\rightarrow}(W) & -\mathbf{D}^{j+1,\leftarrow}(0) & \mathbf{D}^{j+2,\rightarrow}(0) \end{pmatrix} \begin{pmatrix} \boldsymbol{\alpha}^{j,\leftarrow} \\ \boldsymbol{\alpha}^{j+1,\rightarrow} \\ \boldsymbol{\alpha}^{j+1,\leftarrow} \\ \boldsymbol{\alpha}^{j+2,\rightarrow} \end{pmatrix}$$

$$= \begin{pmatrix} -\mathbf{D}^{j,\rightarrow}(0) & 0 \\ 0 & -\mathbf{D}^{j+2,\leftarrow}(0) \end{pmatrix} \begin{pmatrix} \boldsymbol{\alpha}^{j,\rightarrow} \\ \boldsymbol{\alpha}^{j+2,\leftarrow} \end{pmatrix} \tag{18}$$

or

$$\mathbf{D}_{\mathrm{T}}^{\text{out}}\boldsymbol{\alpha}_{\mathrm{T}}^{\text{out}} = \mathbf{D}_{\mathrm{T}}^{\text{in}}\boldsymbol{\alpha}_{\mathrm{T}}^{\text{in}} \tag{19}$$

where $\mathbf{D}_{\mathrm{T}}^{\text{out}}$ is a $4M \times 4M$ matrix, and $\mathbf{D}_{\mathrm{T}}^{\text{in}}$ is a $4M \times 2M$ matrix. The scattering matrix for a tunnelling problem is again defined as in equation (14), so

$$\mathbf{S}_{\mathrm{T}} = (\mathbf{D}_{\mathrm{T}}^{\text{out}})^{-1}\mathbf{D}_{\mathrm{T}}^{\text{in}}. \tag{20}$$

The **S**-matrix for the tunnelling problem is now a $4M \times 2M$ matrix, since the $\alpha^{j+1,\rightarrow}$- and $\alpha^{j+1,\leftarrow}$-coefficients in the barrier, as well as all coefficients of the reflected and transmitted channels are related to the incoming vector α^{in}. The matrix elements of $\mathbf{D}_{\text{T}}^{\text{out}}$ are either of order unity, exponentially small, or zero. Furthermore, there are always matrix elements of order unity on every row or column of $\mathbf{D}_{\text{T}}^{\text{out}}$, implying that inversion of $\mathbf{D}_{\text{T}}^{\text{out}}$ does not give numerical problems (except at singularities of the **S**-matrix as discussed below). The fact that some matrix elements become exponentially small is just a manifestation of the vanishing contribution of an evanescent wave to the matching of the wavefunction at an opposite interface.

Instead of performing the full inversion procedure required for the calculation of the full **S**-matrix (equation (20)) one may alternatively choose a procedure in which the elements of the $\alpha_{\text{T}}^{\text{in}}$-vector in equation (19) are chosen to be all zero, except for one particular incoming wave. It is then numerically easy to solve the set of linear equations given by equation (19), which gives a row of the **S**-matrix.

The above sketched method can also be adopted to treat the QW problem. The incoming channel then corresponds to an evanescent wave decaying towards an interface. Bound states are obtained at energies for which $\det(\mathbf{D}_{\text{T}}^{\text{out}}) = 0$ or, alternatively, for which $\det(\mathbf{S}_{\text{T}})$ has a pole.

3. Envelope functions

Envelope function approaches, as used in the literature all have in common that the envelopes are supposed to fulfil some specific set of equations, together with certain boundary conditions at interfaces. It is not always obvious how reliable either of these are.

What we, in our analysis at least, can do is the following. From the *exact* treatment of scattering (based on empirical pseudopotentials) given previously, we can derive what the related envelope functions are, simply by rewriting our former results in terms of envelope functions. We are then left with envelope functions which are what they ought to be. We are thus in the position to verify whether proposed boundary conditions for envelope functions at interfaces are valid or should be replaced by more appropriate ones.

The envelope functions are introduced as follows (Lüttinger and Kohn 1955): a Bloch-type solution at given energy and $q_{\|}$ is written as

$$\psi^{j,s}(r) = \mathrm{e}^{\mathrm{i}k^{j,s}\cdot r} u^{j,s}(r) = \mathrm{e}^{\mathrm{i}k^{j,s}\cdot r} \sum_n c_n^{j,s} u_{nk_0}^j(r) = \mathrm{e}^{\mathrm{i}(k^{j,s}-k_0)\cdot r} \sum_n c_n^{j,s} \psi_{nk_0}^j(r)$$

$$= \sum_n F_n^{j,s}(r) \psi_{nk_0}^j(r) \tag{21}$$

where $k^{j,s} = q_{\|} + k_z^{j,s} e_z$ and

$$\psi_{nk_0}^j(r) = \mathrm{e}^{\mathrm{i}k_0\cdot r} u_{nk_0}^j(r) \tag{22}$$

is an eigenfunction of the Schrödinger (1) at a fixed point k_0 in the first Brillouin-zone. k_0 is most conveniently chosen to be at an extremum of the bandstructure, like the Γ-point or the X-point. If we restrict ourselves to $q_{\|}$-values and interfaces such that

(see Cuypers and van Haeringen 1991) the envelope functions $F_n^{j,s}(\boldsymbol{r})$, have only one overall factor $e^{i\boldsymbol{q}_\parallel \cdot \boldsymbol{\rho}}$, equation (21) becomes

$$\psi^{j,s}(\boldsymbol{r}) = e^{i\boldsymbol{q}_\parallel \cdot \boldsymbol{\rho}} \sum_n f_n^{j,s}(z)\psi_{n\boldsymbol{k}_0}^j(\boldsymbol{r}) \tag{23}$$

where we have taken $\boldsymbol{k}_{0\parallel} = \boldsymbol{0}$. Note that $f_n^{j,s}(z)$ is in fact equal to $c_n^{j,s}e^{ik_z^{j,s}z}$ (see equation (21)), in which the $c_n^{j,s}$ follow from projecting $u^{j,s}(\boldsymbol{r})$ onto the functions $u_{n\boldsymbol{k}_0}^j(\boldsymbol{r})$. The general wavefunction in a heterostructure layer (3) can now be written as

$$\begin{aligned}\psi^j(\boldsymbol{r}) &= \sum_s^{2M} \alpha^{j,s}\psi^{j,s}(\boldsymbol{r}) = \sum_s^{2M} \alpha^{j,s}e^{i\boldsymbol{q}_\parallel \cdot \boldsymbol{\rho}} \sum_n f_n^{j,s}(z)\psi_{n\boldsymbol{k}_0}^j(\boldsymbol{r}) \\ &= e^{i\boldsymbol{q}_\parallel \cdot \boldsymbol{\rho}} \sum_n \mathcal{F}_n^j(z)\psi_{n\boldsymbol{k}_0}^j(\boldsymbol{r})\end{aligned} \tag{24}$$

with

$$\mathcal{F}_n^j(z) = \sum_s^{2M} \alpha^{j,s} f_n^{j,s}(z)\,. \tag{25}$$

It should be realized that the index n runs from 1 to N, N being the number of energy bands taken into account in our empirical pseudopotential scheme. On the other hand, the number of band-indexed envelope functions taken into account in practical applications of the envelope-function formalism is much lower, and may vary between 1 and 4 (or 8 if spin states are explicitly dealt with). This reduction is generally justified by the application of a Löwdin renormalization procedure (Löwdin 1951), in which it is assumed, among other things, that only a few of the n-dependent terms in (24) significantly contribute to $\psi^j(\boldsymbol{r})$. In such procedures the boundary conditions for envelope functions and their first derivative at $z = z_0$ are most generally expressed in terms of a transfer matrix T

$$\begin{pmatrix} \mathcal{F}^{j+1} \\ \frac{\partial \mathcal{F}^{j+1}}{\partial z} \end{pmatrix} = \mathsf{T} \begin{pmatrix} \mathcal{F}^{j} \\ \frac{\partial \mathcal{F}^{j}}{\partial z} \end{pmatrix} \tag{26}$$

where $\mathcal{F}^j$ now stands for a vector with a few components $\mathcal{F}_n^j(z_0)$ only. Typically, for states in the energy region of the conduction-band minimum one such component could be sufficient. For hole-like states we have at least to include heavy- and light-hole bands. Our approach will be to derive the proper electronic wavefunction for a heterostructure first (as sketched in the previous section), after which we write the obtained solutions in terms of the above introduced envelope functions. We can then check whether or not proposals for the T-matrix given in the literature do satisfy relation (26), in which we substitute the envelope functions as obtained from our calculations.

Although relation (25), based on envelope functions around one $\boldsymbol{k}_0$ only, is formally correct, one might argue that it may not always be equally useful in heterostructures because of the fact that equation (25) generally contains terms corresponding to k_z-values which have a real part not only close to $\boldsymbol{k}_0 = \boldsymbol{0}$ (the Γ-extremum) but close

to $\boldsymbol{k}_0 = \frac{2\pi}{a}\boldsymbol{e}_z$ (the X-extremum) as well. A successful and simple envelope-function theory has always to be combined with Löwdin perturbation theory around a particular extremum. Therefore, dealing more generally with both Γ and X related terms in equation (25), which may be necessary if the energy is close to the energy at an X-extremum, it seems natural to separate the summation into equation (24) into two parts

$$\psi^j(\boldsymbol{r}) = \sum_s^{\Gamma} \alpha^{j,s}\psi^{j,s}(\boldsymbol{r}) + \sum_s^{X} \alpha^{j,s}\psi^{j,s}(\boldsymbol{r})$$

$$= \mathrm{e}^{\mathrm{i}\boldsymbol{q}_\parallel \cdot \boldsymbol{\rho}} \left(\sum_n \mathcal{F}_n^{j,\Gamma}(z)\psi^j_{n\boldsymbol{k}_\Gamma}(\boldsymbol{r}) + \sum_n \mathcal{F}_n^{j,\mathrm{X}}(z)\psi^j_{n\boldsymbol{k}_\mathrm{X}}(\boldsymbol{r}) \right) \tag{27}$$

where the Γ/X index means restriction to solutions corresponding to k_z-values which have a real part close to $\boldsymbol{k}_\Gamma = (0,0,0)$ or $\boldsymbol{k}_\mathrm{X} = (0,0,\frac{2\pi}{a})$. The boundary conditions for such envelope functions and their first derivatives are then expressed as

$$\begin{pmatrix} \mathcal{F}^{j+1,\Gamma} \\ \frac{\partial \mathcal{F}^{j+1,\Gamma}}{\partial z} \\ \mathcal{F}^{j+1,\mathrm{X}} \\ \frac{\partial \mathcal{F}^{j+1,\mathrm{X}}}{\partial z} \end{pmatrix} = \boldsymbol{T}^{\Gamma,X} \begin{pmatrix} \mathcal{F}^{j,\Gamma} \\ \frac{\partial \mathcal{F}^{j,\Gamma}}{\partial z} \\ \mathcal{F}^{j,\mathrm{X}} \\ \frac{\partial \mathcal{F}^{j,\mathrm{X}}}{\partial z} \end{pmatrix}. \tag{28}$$

It is not obvious whether equation (26) is the most suitable or equation (28). Especially when X-related $f_n^{j,s}(z)$-functions in equation (25) are expected to play an important role, as for energies close to the conduction band minimum at the X-point, the latter may be more appropriate. This matter is considered in more detail in section 4.2.

4. Scattering at a single GaAs/AlAs interface

In this section we report on scattering calculations for a single GaAs/AlAs interface. Apart from calculating amplitudes for outgoing channels we also derive the related envelope functions and discuss their apparent connection rules.

4.1. Empirical pseudopotential calculations

The complex bandstructures of the materials GaAs and AlAs have been calculated using the same procedure as Chang and Schulman (1982), and using the pseudopotential form-factors as given by Baldereshi *et al* (1977). The constants U_0^j in (1) are taken such that the valence band offset is equal to 35% of the difference in the bandgap of material j and $j+1$. We have used 59 plane waves in our calculation leading to 42 k_z-solutions ($M = 21$). In figure 2 we have plotted the positive value of the real and imaginary parts of these k_z-solutions as a function of energy, for $\boldsymbol{q}_\parallel = \boldsymbol{0}$. In order to follow the branches with a real part in the vicinity of the X-point continuously as a function of energy, the 1BZ in the k_z-direction is chosen to lie between $\frac{-\pi}{2a}$ and $\frac{3\pi}{2a}$.

For the incident wave we have chosen the channel in GaAs, corresponding to a light-hole for energies in the valence band regime, and an electron for energies in the conduction band regime. In the energy gap of GaAs we choose as the incoming channel the evanescent state corresponding to the branch connecting the light-hole band with

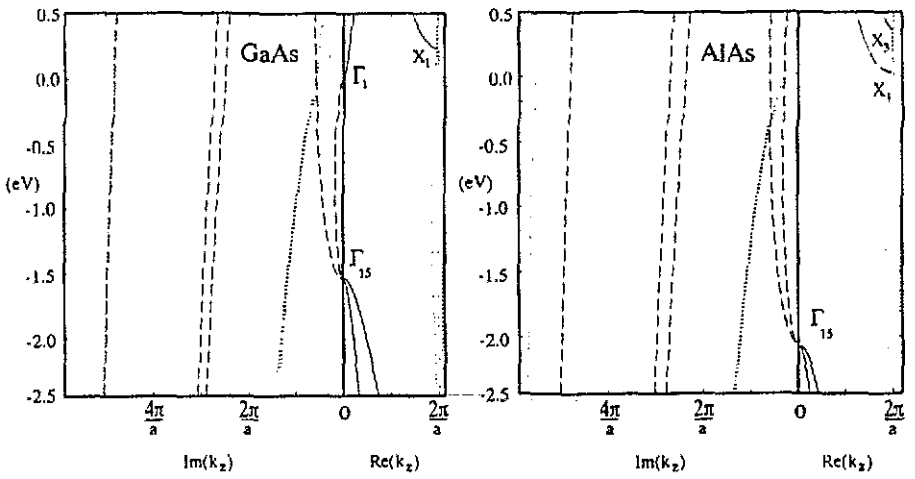

Figure 2. Complex bandstructures of GaAs and AlAs at $q_{\|} = 0$. The zero of energy corresponds to the conduction-band minimum of GaAs. The positive real part of the k_z-values is plotted at the right of the zero axis, the positive imaginary part is plotted at the left of the zero axis. Purely real k_z-values are denoted by solid curves, purely imaginary k_z-values by broken curves, and complex k_z-values by dotted curves. The complex k_z-values which have a real part slightly deviating from $2\pi/a$ correspond to the branches which are connected to the X-minima of the first and second conduction-band.

the conduction band. In a heterostructure with a single interface this channel would of course be prohibited, as it is evanescent towards the interface, but in configurations with multiple interfaces it may be allowed. In order to obtain an impression of the relevance of the 21 outgoing channels in GaAs as well as the 21 for AlAs we have plotted in figure 3 the maximum values which each of the 42 α_s^{out}-coefficients assume in the considered energy interval. The actual α_s^{out}-values at one given energy may of course be quite different from those in figure 3, but as intuitively expected, the reflected and transmitted light-hole/electron are most important, but also the heavy-holes and, to a lesser extent, the solutions with a real part of k_z close to the X-point may play a significant role. Also, certain evanescent states (for instance channel 7) are not entirely negligible. The absolute values of the most important $\alpha^{j,s}$-coefficients are plotted as a function of energy in figures 4–6. The most striking features are the resonances of the light-hole and heavy-hole $\alpha^{j,s}$-coefficients at energies just above the valence-band edges of AlAs and GaAs. We explain these resonances as the tendency of the system to form an interface state. Such an interface state would exist if the determinant of the matrix $\mathbf{D}^{\text{out}}$ (see equation (13)) were zero. At the resonant energies, the absolute value of this determinant, which is plotted in figure 7, shows sharp dips, indicating that there is an almost perfect match of the wavefunction consisting of outgoing channels only. The effects of the electrostatic potential connected with such interface states have not been accounted for in our calculations. Furthermore, the locations of the resonances are at the valence-band edges of AlAs and GaAs, for which the effects of the spin–orbit interaction are important. A calculation incorporating both the electrostatic potential and spin-orbit interaction would therefore be necessary to study these resonances in full detail.

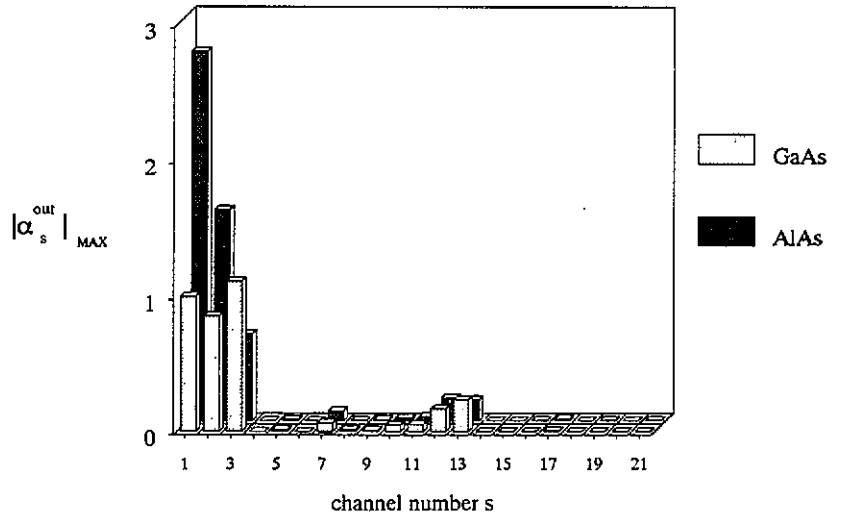

Figure 3. The maximum of the absolute value of the α^{js}-coefficients of each outgoing channel s in the energy range -2.5 eV to 0.5 eV, for the case of an incoming light-hole/electron. The use of 59 plane waves in the calculation gives rise to 21 outgoing channels in each material layer. The channel number $s = 1$ corresponds to the reflected/transmitted light-hole/electron states. The numbers $s = 2$ and $s = 3$ correspond to the twofold degenerate heavy-hole states. The channel numbers above $s = 11$ correspond to k_z-values with a real part close to $2\pi/a$. The numbers $s = 12$ and $s = 13$ correspond to branches which are, more specifically, connected to the X-minima of the first and second conduction-band, respectively.

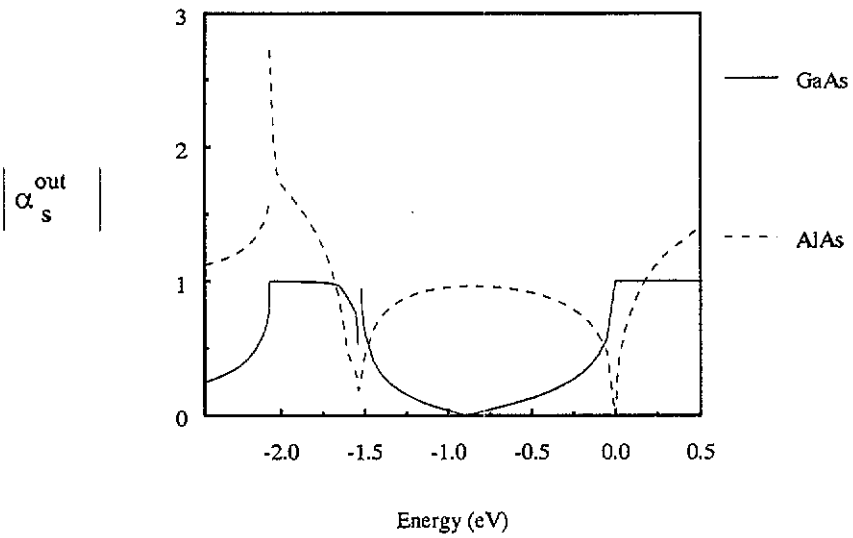

Figure 4. The absolute value of the α_3^{out}-coefficients corresponding to the reflected light-hole/electron in GaAs (solid curve) and the transmitted light-hole/electron in AlAs (broken curve) as a function of energy. The sharp peaks occur just above the valence band edges of GaAs and AlAs, respectively.

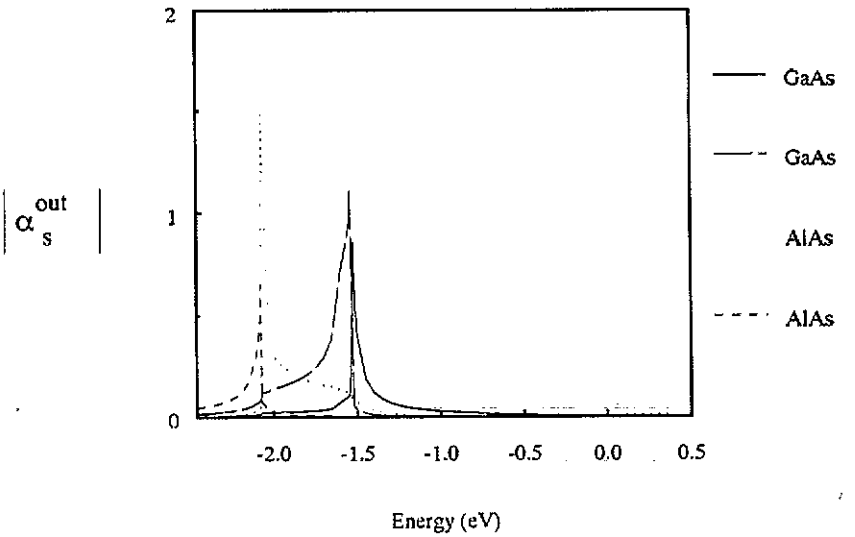

Figure 5. The same as in figure 4, but now for the heavy holes in GaAs and AlAs, which are twofold degenerate at $q_{\|} = 0$.

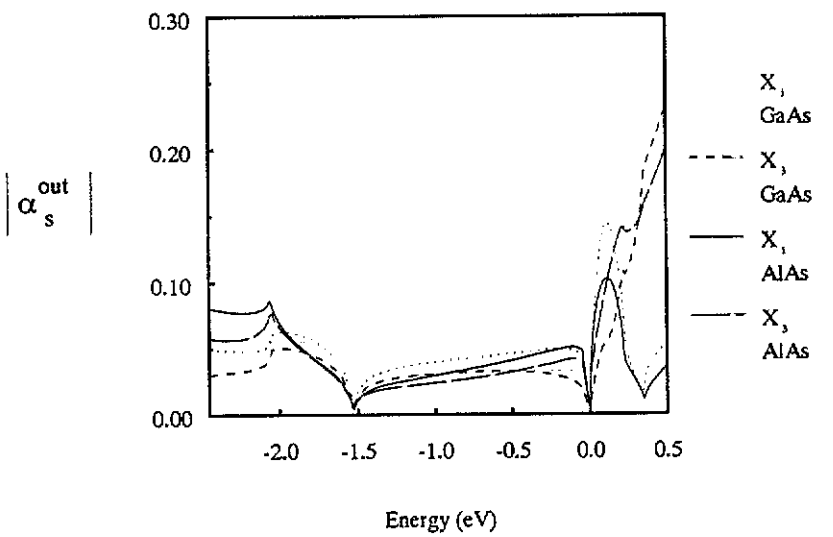

Figure 6. The same as in figure 4, but now for the complex k_z-branches which are connected to the X-minimum of the first conduction band (X_1) and the second conduction band (X_3) of GaAs and AlAs.

As can be seen in figure 6, the solutions associated with the X-point are not negligible, especially in the important conduction-band regime. They may constitute about 10–20% of the total wavefunction at the interface. However, if one is interested in charge densities or fluxes carried by these states (for energies above the X-minimum) their importance is only minor, since the charge density and flux are proportional to $|\alpha^{j,s}|^2$, which is about 1–4% of the total charge or flux. This is not to say that the incorporation of X-states in the theory is unnecessary, as they may play an important

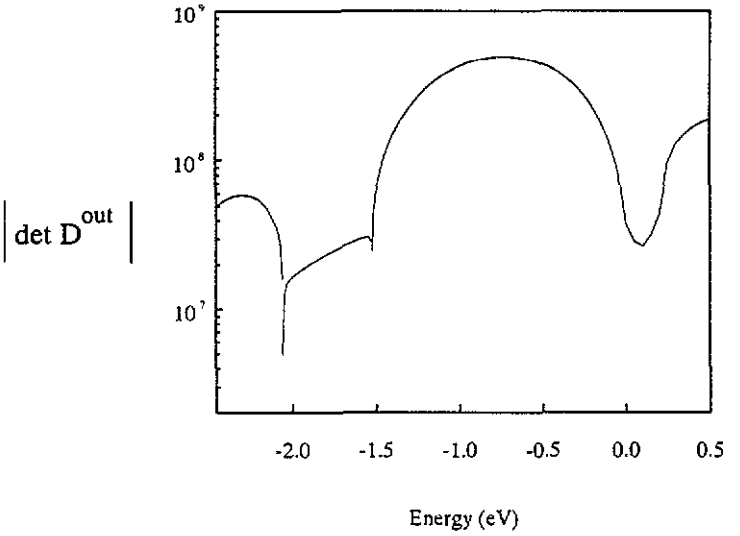

Figure 7. The absolute value of the determinant of the matrix $\mathbf{D}^{\mathbf{out}}$ (see equation (19)). The sharp dips are positioned at the same energies as the peaks in figure 4. A zero in the determinant is likely to correspond with an interface state.

role in the matching at an interface, by fixing the actual values of the coefficients $\alpha^{j,s}$ for Γ-states, say.

4.2. Connection rules for envelope functions

Having calculated the $\alpha^{j,s}$-coefficients, we are now able to calculate the envelope functions $\mathcal{F}_n^j(z)$, using equation (25). We will focus on the energy region above the Γ conduction band minimum in GaAs. At these energies the most important $\alpha^{j,s}$-coefficients, for the case of an incident Γ-electron, are the ones which correspond to the transmitted and reflected Γ-electron, the absolute values of which are given in figure 4. The most dominant functions $f_n^{j,s}(z)$, belonging to these $\alpha^{j,s}$-coefficients, are the ones with the band index $n = c$ of the conduction band, since their $k_z^{j,s}$-values are close to the conduction band minimum at the Γ-point of GaAs and AlAs, although we find from our calculations that these functions are also significant for the light-hole valence band ($n = lh$). We will therefore consider the **T**-matrix connecting the conduction and light-hole band envelope functions $\mathcal{F}_c^j(z)$ and $\mathcal{F}_{lh}^j(z)$ in GaAs and AlAs, which then obviously reduces to a 4×4 matrix (see equation (26)). We remark that most, if not all, connection prescriptions in the literature for electron states in the considered energy region are formulated in terms of a diagonal 2×2 **T**-matrix, connecting the $\mathcal{F}_c(z)$-functions only. Our calculations enable us to determine the actual values of any of these diagonal **T**-matrix elements as functions of energy. In figure 8 the **T**-matrix elements T_{cc} and $T_{lh,lh}$, connecting the $\mathcal{F}_c$ and $\mathcal{F}_{lh}$-functions, are given as functions of energy (note that T_{cc} and $T_{lh,lh}$ can be chosen to be real). A striking feature is that $1 < T_{cc} < 1.004$, and $0.995 < T_{lh,lh} < 1.003$ for a relatively large energy interval (0.5 eV) above the Γ-conduction band minimum in GaAs. This implies that the envelope function $\mathcal{F}_c(z)$ as well as $\mathcal{F}_{lh}(z)$ can indeed be considered to be almost perfectly continuous at an interface, which supports the connection rule for the conduction-band envelope function as is often used in the literature. We remark

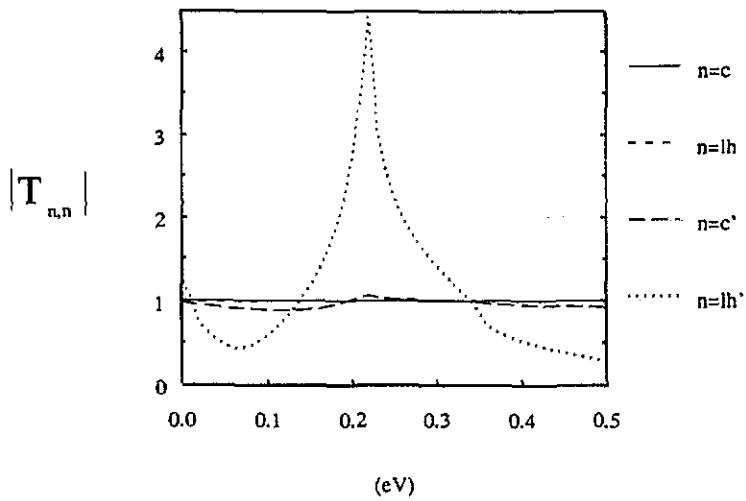

Figure 8. Absolute value of the diagonal elements of the transfer matrix **T**, relating envelope functions and their first derivatives at the two sides of an interface. Accents at band indices denote transfer matrix elements between the first derivatives of the envelope functions.

that the small deviations of T_{cc} and $T_{lh,lh}$ from 1 are not due to numerical inaccuracies.

The absolute values of the $T_{c'c'}$ and $T_{lh',lh'}$-matrix elements, being the elements relating the first derivatives of the envelope functions $\mathcal{F}_c(z)$ and $\mathcal{F}_{lh}(z)$ at an interface, are also plotted in figure 8. What is again striking is that the first derivative of the envelope function $\mathcal{F}_c(z)$ is approximately continuous as well. The deviations of $T_{c'c'}$ from unity are within 10–15%. However, this is in contradiction with the often applied rule that $T_{c'c'} = m^*_{j+1}/m^*_j$ which would be equal to about 3 for a GaAs/AlAs-based heterostructure! The $T_{lh',lh'}$-matrix element, in contrast to $T_{c'c'}$, is far from being constant in this energy range, implying that $\partial\mathcal{F}_{lh}/\partial z$ is not at all continuous at the interface. On the contrary, its mismatch in continuity is rather strongly dependent on energy. It is worthwhile to re-emphasize that we did not assume the basis functions $\psi^j_{n0}(\boldsymbol{r})$ (see equation (21)) to be identical for both materials, as is a common *ansatz* in the literature, but have taken the exact eigenfunctions of the Schrödinger equation (1) at $k_0 = 0$ for each material. We again stress that the envelope functions which have been used to obtain the **T**-matrix elements are the exact ones, and are not obtained from an approximate set of Löwdin renormalized envelope-function equations. Note in this connection that the envelope functions we are considering contain all $2M$ terms as given by equation (25).

The envelope function $\mathcal{F}^j_c$ considered above, is composed of a variety of $f^{j,s}_c(z)$-functions ($2M$ in total), including the functions which are related to $k^{j,s}_z$-values which have a real part close to the X-point. (Similarly $\mathcal{F}^j_{lh}$ is composed of a variety of $f^{j,s}_{lh}(z)$-functions.) As we have observed in figure 6, the $|\alpha^{j,s}|$ belonging to such X-related solutions are relatively small. However, in considering $\partial\mathcal{F}^j_n/\partial z$ we have to realize that $\partial f^{j,s}_n/\partial z$-values related to $k^{j,s}_z$-values close to the X-point may be much more important than those related to $k^{j,s}_z$-values close to the Γ-point, as they contribute proportionally to $k^{j,s}_z\alpha^{j,s}$ instead of $\alpha^{j,s}$. This implies that the contribution to $\partial\mathcal{F}^j_n/\partial z$ of X-related $\partial f^{j,s}_c/\partial z$-functions may very well be of equal importance as the

contribution of the Γ-related $\partial f_n^{j,s}/\partial z$-functions. In addition, if the real part of $k_z^{j,s}$ is close to X, we have to face the fact that the related $f_n^{j,s}$-functions are significant for a relatively large set of n-values. This is due to the Lüttinger–Kohn procedure in which $\psi_k^{j,s}(r)$-functions are expanded in terms of $\psi_{n,k_0}^{j}(r)$-functions with $k_0 = 0$ (equation (21)). In order to avoid too many n-values playing a significant role, it might be more convenient to separate the summation over the $2M$ terms in (25) into two parts as in equation (27). In that way envelope-function expansions of $\psi_k^{j,s}(r)$-functions with k_z close to $k_{0z} = \frac{2\pi}{a}$ require only a few band indices, and the first derivatives of $f_n^{j,s}(z)$-functions corresponding to these solutions become proportional to $(k_z - k_{0z})\alpha^{j,s}$. For the most important $\alpha^{j,s}$-coefficients, corresponding to solutions with $k_z^{j,s}$-values close to the X-minimum of the conduction band, for which the absolute values are given in figure 6, the $f_n^{j,s}$-function with the conduction band index $n = c$ will again be the dominating one, although also the second conduction band $n = c_2$ may play a comparable role.

Whether this separation in Γ- and X-related envelope functions will then lead to more transparent envelope-function descriptions remains of course to be proven, but we are again in the position to verify what the connection rules for such separated envelope functions actually are. To this end we have carried through the above described separation in Γ- and X-related $f_n^{j,s}(z)$-functions (see equation (27)) and have actually calculated the above introduced $\mathcal{F}_n^{\Gamma}(z)$, for $n = c$ and $n = lh$, and $\mathcal{F}_n^{X}(z)$, for $n = c$ and $n = c_2$. The $T^{\Gamma,X}$ matrix connecting the $\mathcal{F}_c^{\Gamma,X}$, $\mathcal{F}_{lh}^{\Gamma}$ and $\mathcal{F}_{c_2}^{X}$-envelope functions and their first derivatives becomes an 8×8 matrix. For the moment we are especially interested in the effect of the separation in Γ- and X-related terms on the connection rules for the remaining Γ-related envelope functions $\mathcal{F}_c^{\Gamma}$ and $\mathcal{F}_{lh}^{\Gamma}$. The newly defined T_{nn}^{Γ}-matrix elements for $n = c$ and $n = lh$, connecting $\mathcal{F}_c^{\Gamma}$ and $\mathcal{F}_{lh}^{\Gamma}$, as well as the absolute value of the $T_{n',n'}^{\Gamma}$-matrix elements for $n = c$ and $n = lh$, connecting the first derivatives of $\mathcal{F}_c^{\Gamma}$ and $\mathcal{F}_{lh}^{\Gamma}$, are given as a function of energy in figure 9. These matrix elements are again approximately constant and nearly equal to 1, with $0.945 < T_{cc}^{\Gamma} < 0.956$ and $0.969 < T_{lh,lh}^{\Gamma} < 0.986$. So again, both the $\mathcal{F}_c^{\Gamma}$ and $\mathcal{F}_{lh}^{\Gamma}$-envelope functions are approximately continuous at the interface, although this approximation is somewhat worse than it is for the unseparated envelope functions. The first derivative of $\mathcal{F}_c^{\Gamma}$ is again approximately continuous at the interface, with $|T_{c',c'}^{\Gamma}| = 1.26 \pm 0.10$. The value of $|T_{c',c'}^{\Gamma}|$ is still far from the ratio of the effective masses of AlAs and GaAs, so the separation in Γ- and X-related terms does not remove the discrepancy between our results and the m_{j+1}^*/m_j^*-rule for connecting the first derivative of the conduction-band envelope function. The absolute value of the $T_{lh',lh'}^{\Gamma}$-matrix element has a very strong dependence on the energy. There is no improvement on the case in which we did not perform a separation in Γ- and X-related terms. On the contrary, the value of $|T_{lh',lh'}^{\Gamma}|$ varies as much as two decades in the energy interval under consideration. There is, therefore, apparently no simple connection rule for the $\partial \mathcal{F}_{lh}/\partial z$-function in this energy range.

The $\mathbf{T}^{X}$-matrix elements for $n = c$ and $n = c_2$ appear to have no simple dependence on energy. The problem concerning the connection of X-related envelope functions at interfaces will be addressed in a future paper.

5. Application to a GaAs/AlAs/GaAs single barrier structure

Having dealt with the case of a heterostructure with one interface only, we are now

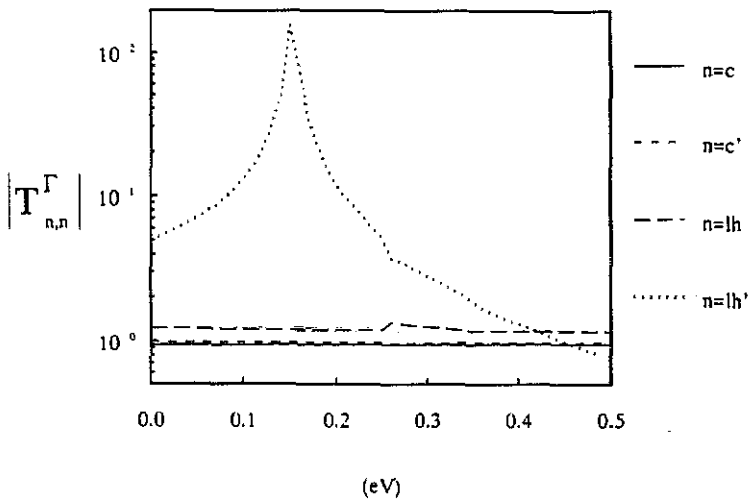

Figure 9. The same as figure 8, but now for Γ-related envelope functions (see main text).

ready to deal with a heterostructure consisting of three material layers, separated by two interfaces. We will use the method as developed in section 2, based on empirical pseudopotentials. We also will use an envelope function approach, in which we will apply some of the results of the previous section with respect to the boundary conditions for the envelope functions and their first derivatives.

We consider a GaAs/$Al_xGa_{1-x}As$/GaAs single barrier structure, with $x = 1$ and $x = 0.3$. Although, in principle, we are also capable of dealing with the $Al_xGa_{1-x}As$/GaAs/$Al_xGa_{1-x}As$ quantum well problem, we will not do so, for we have not yet incorporated spin-orbit interaction which is of importance for the hole-bound states. The $x = 1$ case is particularly interesting, since AlAs is an indirect semiconductor. The situation is such that the AlAs layer acts as a barrier for Γ-electrons, whereas the X-electrons see the AlAs layer as if it were a potential well. At the interface there will be a coupling between Γ- and X-electrons, as we have seen in section 4.1, so the X-valley assisted transmission of a Γ-electron through the AlAs layer may play an important role. In this view, it is important that the bandstructure around the X-point is calculated accurately. We therefore calculate the complex bandstructure around the Γ-point and X-point separately, using sets of reciprocal lattice vectors, which lie in shells around the Γ- and X-point, respectively. The position of the conduction band minimum at the X-point with respect to the minimum at the Γ-point is taken from experimentally obtained values (Casey and Panish 1978). All other parameters are the same as those given in section 2. We consider a tunnelling structure with a barrier thickness of 20 monolayers which is equal to 56.6 Å. Corresponding to the 27/32-plane wave basis set, there are 13 $\boldsymbol{G}$-vectors, which lead to 26 k_z-solutions which are taken into account. However, in dealing with the connection problems at the two interfaces (see section 2) we have the option of reducing the number S of k_z-solutions to be taken into account by simultanuously reducing the number M' of $\boldsymbol{G}$-vectors, such that $S = 2M'$. Since the $\boldsymbol{G}$-vectors are arranged in shells, it is quite natural to choose the number M' to be equal to 13 (i.e. taking them all into account) or equal to the reduced values 9, 5 or 1, respectively. For these four values of M'

we have calculated, for an incoming Γ-electron, the amplitude of the Bloch-function, corresponding to the transmitted Γ-electron (which we denote by α_t). Note that for each of the above four sets of G-vectors the appropriate k_z-solutions have been taken into account, following from the full 27/32-plane wave basis set calculation. We have also calculated the transmission coefficient α_t according to an approximation in which $M' = 1$ and in which the periodic parts $u_k(r)$ of the involved Γ-band Bloch solutions $e^{ik \cdot r} u_k(r)$ are taken to be constant ($u_k(r) \equiv 1$), while the remaining envelope functions and their first derivative are assumed to be continuous at the interfaces.

The absolute values of the α_t-coefficients for $x = 1$, as obtained for all these cases, are plotted in figure 10 as functions of energy. What is particularly striking is the large number of resonances in the transmission amplitude of the Γ-electron. These resonances are related to bound states of the X-electrons in the quantum well, formed by the X-valley band edges of GaAs and AlAs. Even more striking is the occurrence of anti-resonances (a very strong one lying at 0.38 eV), where the transmission amplitude drops to zero. Such results were already obtained earlier by Ko and Inkson (1988). They have pointed out that these anti-resonances may be explained by the Fano theory (Fano 1961), which describes the behaviour of a resonance coupled to a continuum of scattering modes. Clearly the correct α_t-coefficient, as obtained by taking the full number of 13 G-vectors into account, is already obtained if only 9 G-vectors instead of 13 are taken into account. Also, 5 G-vectors already leads to very reasonable results. This rapid convergence is due to the fact that the contribution of evanescent states with a relatively large imaginary part of k_z is relatively unimportant. These are the ones that are accounted for if 9 G-vectors or more are used. Using only one G-vector for the calculation of the α_t-coefficient, fails drastically. This is due to the fact that the $u_k(r)$-functions can only reasonably well be represented by at least five 2D Fourier coefficients. The envelope-function approximation (see the curve denoted by $u(r) = 1$) clearly is not able to describe the resonances due to tunnelling through the X-valley in AlAs, but appears to be a reasonably good approximation for the background tunnelling probability, due to tunnelling through the Γ-barrier. At energies below the X-minimum in AlAs the envelope-function approximation underestimates the transmission amplitude, but at energies close to the Γ-conduction band edge of AlAs it is a fairly good approximation to the exact transmission amplitude.

The results for $x = 0.3$, for which $Al_xGa_{1-x}As$ is a direct semiconductor, are given in figure 11. At 0.46 eV there is a small peak, which is due to the first resonant tunnelling mode through the X-valley. It is obvious that using only 1 G-vector again fails, but that using five G-vectors already leads to the correct result for the transmission amplitude. It is observed that the envelope-function approximation with $u_k(r) \equiv 1$ is very accurate. We remark that in this approximation the k_z-values for the Γ-bands involved follow from our full EPM bandstructure calculations. We have compared these results with three more types of envelope-function approximations. Firstly, we consider an envelope-function approach, in which there is supposed to be one uniform effective mass for the GaAs and $Al_xGa_{1-x}As$ Γ-bands throughout the whole structure, being the effective mass of GaAs (as obtained from the EPM calculation). Only k_z-values for these Γ-bands are considered. The k_z-values follow from $E = \hbar^2 k_z^2 / 2m^*$ ($q_{\|} = 0$), where m^* is the effective mass (at $k_0 = 0$) as obtained from the EPM calculations. The envelope functions and their first derivatives are continuous at the interface. Secondly, we have taken the approximation in which we used two such effective masses, one for each material, and where the envelope function and its first derivative are again taken to be continuous at the interface. Note that this approxi-

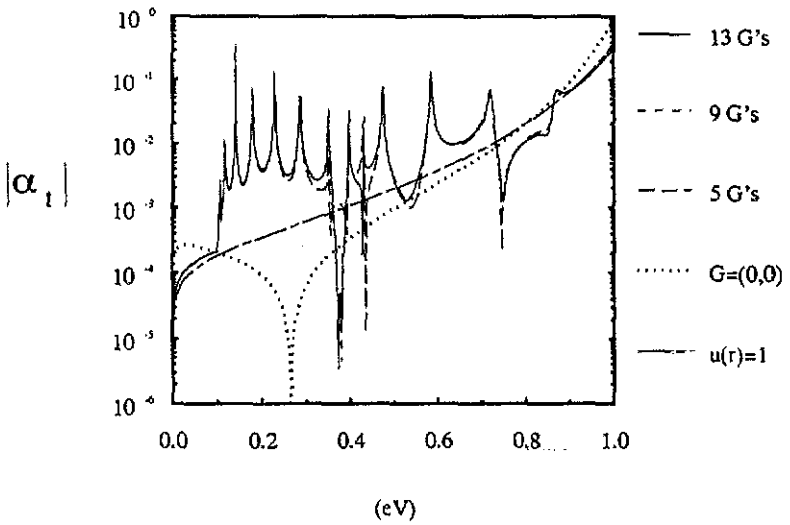

Figure 10. The absolute value of the amplitude α_t of the transmitted Γ-electron through an AlAs barrier in a GaAs-crystal, calculated using 13, 9, 5 or 1 2D reciprocal lattice vectors G. Also the case in which the periodic part of the Bloch functions $u(r)$ is put equal to 1 is given. The (anti-)resonant peaks are due to resonant tunnelling through the X-valley of AlAs.

mation differs from our above $u_k(r) = 1$ approximation as the k_z-values involved are determined differently. The third approach again uses two effective masses, but now the first derivative is discontinuous, the discontinuity being governed by the ratio of the effective masses. The results of these calculations are plotted in figure 12, together with our earlier 13 G-vectors result. All three approximations give reasonably good results for the transmission amplitude. That closest to the exact result is the third approach, which uses a discontinuity in the first derivative of the envelope function governed by the effective mass ratio. However, this latter result, which is at variance with the results in section 4.2 for $x = 1$ should not be overemphasized in the $x = 0.3$ case, the reason being that the ratio of the effective masses is about 0.8 in this case, i.e. relatively close to 1. The relative success of the third approach therefore, can certainly not be interpreted as a general plea for a connection rule for derivatives of envelope functions involving effective mass ratios.

6. Discussion and concluding remarks

In this paper we have treated the matching problem of the electronic wavefunction at a GaAs/AlAs interface, by carefully accounting for contributions of Bloch and evanescent states. We have done this in the framework of the flat-band approximation, on the basis of an empirical pseudopotential approach. It is shown that evanescent states with a large imaginary part of k_z ($\mathrm{Im}(k_z) > 2\pi/a$) do not play a significant role in the matching problem. Solutions which have a real part of k_z, close to the X-point, which can be related to the minimum of the first and second conduction band at the X-point, however, do play a non-negligible role in the matching of the electronic wavefunction at the interface. Especially for energies near the minimum of the conduction band at the X-point, these X-states should therefore be accounted for in the calculations of electronic states in heterostructures.

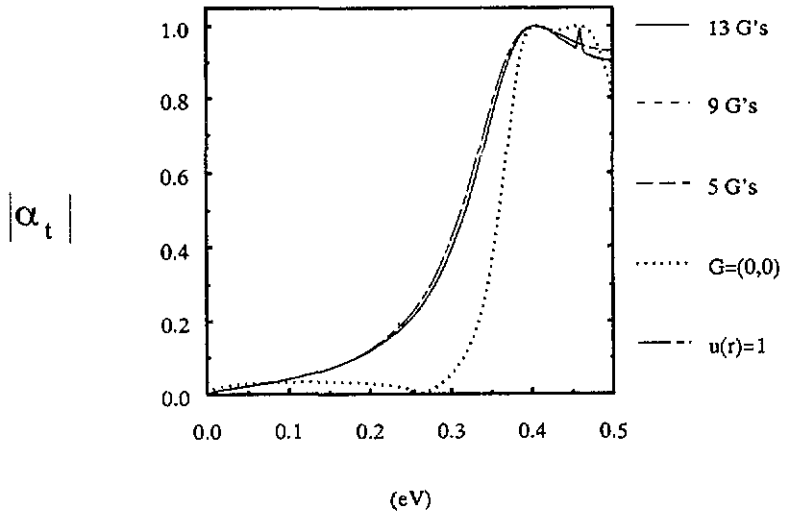

Figure 11. The same as figure 10, but now for an $Al_{0.3}Ga_{0.7}As$-barrier in GaAs. The curves corresponding to 13, 9 and 5 G-vectors overlap each other.

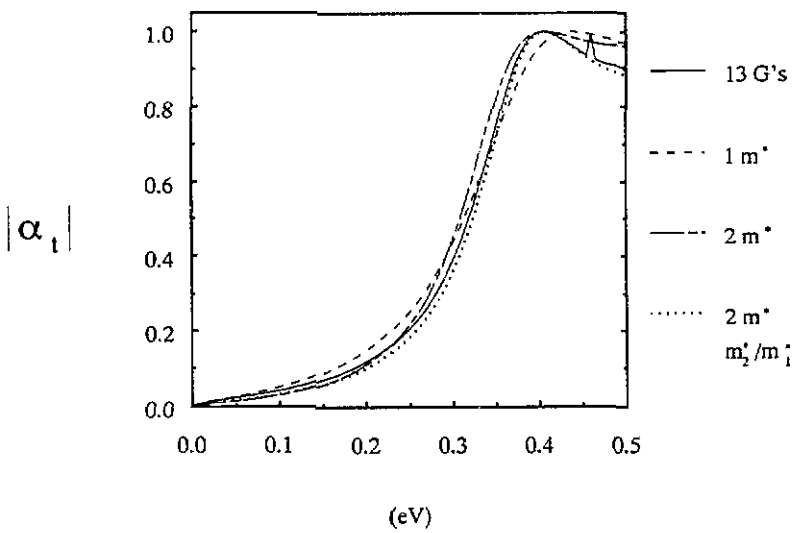

Figure 12. The same as figure 11, but now calculated using envelope-function approaches in which one (shortly dashed curve) or two (long dashes) effective masses are used, using continuous envelope functions and first derivatives. The approach in which the first derivative is discontinuous, governed by the effective mass ratio, is denoted by the dotted curve. Also the exact result (using 13 G-vectors) is given (full curve).

Using the obtained wavefunction we have calculated the corresponding envelope functions. These functions usually follow from Löwdin renormalized envelope-function equations like, for instance, the widely used effective mass equation. But here we deduce them directly from the true wavefunction. It appears, for energies in the important conduction-band region, that only the conduction and light-hole band en-

velope functions are non-negligible. Both the conduction band and light-hole band envelope functions appear to be almost perfectly continuous at the interface, which is in accordance with connection rules for envelope functions as used in the literature. However, when regarding the first derivative of the envelope functions, we also find an approximate continuity for the first derivative of the conduction-band envelope function, which clearly contradicts the often applied $m^*_{\mathrm{AlAs}}/m^*_{\mathrm{GaAs}}$-rule. The first derivative of the light-hole envelope function is found not to obey a simple connection rule; the ratio of this derivative in GaAs and AlAs appears to be strongly dependent on energy. We want to emphasize that we have checked afterwards that the obtained envelope functions and their first derivatives have indeed been constructed in such a way that the corresponding true wavefunction and first derivative are continuous at every x, y-point of the interface. Of course the current density probability will then be continuous as well. Though it is tempting to state that the above deviation from the $m^*_{\mathrm{AlAs}}/m^*_{\mathrm{GaAs}}$-rule will be a general result for all cases, we have to realize that this result is obtained for envelope functions as defined according to (21), i.e. related to the basis functions $\psi^j_{n\boldsymbol{k}_0}(\boldsymbol{r})$ of the respective sublayers j. We suggest that for this choice of envelope functions, the above obtained boundary conditions might very well be a general result, though more numerical evidence could be of help in settling this point. It should be realized, however, that the ambiguity in the choice of the basis functions makes the set of envelope functions ambiguous as well. Depending on the specific choice, the boundary conditions will, consequently, be different. It therefore remains to be investigated whether the above observed discrepancy with the generally applied $m^*_{\mathrm{AlAs}}/m^*_{\mathrm{GaAs}}$-rule could be attributed to this ambiguity, or to an inherent weakness of the effective mass theory.

A successful envelope function theory is always combined with Löwdin renormalization. In the light of this we have separated the envelope-function expansion of the electronic wavefunction for the heterojunction into two parts: one corresponding to envelope functions related to the Γ-valley and the other to envelope functions related to the X-valley. Each type of envelope function can then be approximately calculated using more simple Löwdin renormalized envelope-function equations around the Γ- and X-point, respectively. We have verified whether such Γ-envelope functions of this separated kind satisfy simple connection rules or not. Again, it appears that both the conduction band and light-hole band Γ-type envelope functions are almost continuous at the interface, although the deviations from continuity are slightly larger than in the previous case. The first derivative of the conduction band envelope function also obeys a simple connection rule, although the ratio between the first derivative in AlAs and GaAs now appears to be 1.26 ± 0.10. This is again not equal to the ratio of the effective masses of AlAs and GaAs. The connection rule for the first derivative of the Γ-related light-hole envelope function has become even more dependent on energy. The above separation procedure is therefore not successful in leading to simpler connection rules.

The empirical pseudopotential method has been applied to the tunnelling of an incident Γ-electron through an $\mathrm{Al}_x\mathrm{Ga}_{1-x}\mathrm{As}$ barrier, with either $x = 1$ or $x = 0.3$, in a GaAs crystal. We have presented a numerical stable method for calculations to deal with this two-interface problem, also for very large barrier widths. The result for the transmission probability of a Γ-electron through an AlAs barrier shows strong resonant peaks, which are due to resonant transmission through bound states of X-electrons in the X-valley quantum well formed in the GaAs/AlAs/GaAs structure. Apart from these resonances, strong anti-resonances are found, in which the transmission amplitude is lower than the background transmission amplitude, due to

tunnelling through the Γ-barrier. It can even drop to nearly zero. The calculations were shown to converge rapidly as a function of the number of 2D reciprocal lattice vectors. This is undoubtedly of importance in future calculations on structures with multiple interfaces, like superlattices, in view of both computing time and memory requirements. For the $Al_{0.3}Ga_{0.7}As$ barrier the transmission probability is dominated by the tunnelling of Γ-electrons through the barrier. The X-type solutions appear to play a negligible role for the transmission probability. We have compared our EPM obtained results for the transmission through the above two types of barrier ($x = 1$ and $x = 0.3$) with results obtained from simple envelope-function approximations. For the $x = 1$ case, the envelope-function approach fails for energies above the X-minimum in AlAs, due to the neglect of resonant tunnelling through X-states. Below this energy the envelope-function approach is reasonable; it underestimates the transmission amplitude by about 15–20%. For the $x = 0.3$ case the Γ-band transmission turns out to be reasonably well described by the envelope-function approaches throughout the whole energy range above the conduction band minimum in GaAs and below the Γ-minimum in AlAs. Calculations for heterostructures involving more than two interfaces, as well as the quantum well problem for hole states (for which spin–orbit interaction will be included) will be dealt with in a forthcoming paper.

Acknowledgments

We are greatly indebted to Dr C Van de Walle who put the data presented in figure 1 at our disposal. This work is part of the research program of the 'Stichting voor Fundamenteel Onderzoek der Materie (FOM)', which is financially supported by the 'Nederlandse organisatie voor Wetenschappelijk Onderzoek (NWO)'.

Appendix. Number of k_z-solutions

We start by considering the $2N$ k_z-solutions at given $q_\parallel$ and energy E for the empty lattice case. The k_z-solutions follow from

$$\prod_{m=1}^{N}\left[(q_\parallel + k_z e_z + K_m)^2 - \frac{2mE}{\hbar^2}\right] = 0 \tag{A1}$$

or (with $K_m = G_m + G_{m,z}e_z$)

$$k_z = -G_{m,z} \pm \sqrt{\frac{2mE}{\hbar^2} - (q_\parallel + G_m)^2}\,. \tag{A2}$$

Clearly each G_m component gives rise to a number of k_z-values, two for each $G_{m,z}$-value. These $G_{m,z}$-values are equidistantly distributed and count precisely the number of K_m-vectors at given G_m. *At most* one $G_{m,z}$-value will be given by $q_\parallel + \mathrm{Re}(k_z)e_z \in$ 1BZ. If such a k_z-value exists we have in fact identified a k_z, either belonging to a true Bloch wave (k_z real) or a truly evanescent wave (k_z complex), the other k_z merely differing by a reciprocal lattice vector. The possibility also exists that no such k_z-value exists at a given G_m. In that case, it will always be possible, however, to reduce the members of the related set of vectors $q_\parallel + k_z e_z$ to a vector $q_\parallel + G_i + k_z e_z \in$ 1BZ, where

G_i is one specific member of the set of two-dimensional reciprocal lattice vectors G_m. This shows that the number of k_z-values to be retained in the empty lattice case is indeed equal to twice the number of G_m-vectors, which is $2M$ instead of $2N$. We now argue on the basis of continuity, that the above result not only holds for the empty lattice case, but also for a finite potential case. Note that our result was previously obtained by V Heine (1963).

References

Altarelli M 1983 *Phys. Rev.* B **28** 842
Ando T, Wakahara S and Akera H 1989 *Phys. Rev.* B **40** 11609
Baldereschi A, Hess E, Maschke K, Neumann H, Schulze K R and Unger K 1977 *J. Phys. C: Solid State Phys.* **10** 4709
Baldereschi A, Baroni S and Resta R 1988 *Phys. Rev. Lett.* **61** 734
Bastard G 1981 *Phys. Rev.* B **24** 5693
Brand S and Hughes D T 1987 *Semicond. Sci. Technol.* **2** 607
Burt M G 1989 *Band Structure Engineering in Semiconductor Microstructures* (New York: Plenum)
Casey H C Jr and Panish M B 1978 *Heterostrucure Lasers* (New York: Academic) Part A
Chang Y and Schulman J N 1982 *Phys. Rev.* B **25** 3975
Cohen M L and Bergstresser T K 1966 *Phys. Rev* **141** 789
Cuypers J P and van Haeringen W 1991 *Physica* B **168** 58
Edwards G and Inkson J C 1990 *Semicond. Sci. Technol.* **5** 1023
Eppenga R, Schuurmans M F H and Colak S 1985 *Phys. Rev.* B **36** 1554
Fano U 1961 *Phys. Rev.* **124** 1866
Heine V 1963 *Proc. Phys. Soc.* **81** 300
Hurkx G A M and van Haeringen W 1985 *J. Phys. C: Solid State Phys.* **18** 5617
Kane E O 1982 *Handbook on Semiconductors* vol 1 (Amsterdam: North-Holland) p 193
Ko D Y K and Inkson J C 1988 *Phys. Rev.* B **38** 9945
Lüttinger J M and Kohn W 1955 *Phys. Rev.* **97** 869
Löwdin P 1951 *J. Chem. Phys.* **19** 1396
Marsh A C and Inkson J C 1986 *Semicond. Sci. Technol.* **1** 285
Mott N F and Jones H 1936 *The Theory of the Properties of Metals and Alloys* (Oxford: Clarendon)
Pickett W E, Louie S G and Cohen L 1978 *Phys. Rev.* B **17** 815
Pötz W and Ferry D K 1987 *Superlatt. and Microstr.* **3** 57
Schuurmans M F H and 't Hooft G W 1985 *Phys. Rev.* B **31** 8041
Smith D L and Mailhiot C 1986 *Phys. Rev.* B **33** 8345
Van de Walle C G and Martin R M 1987 *Phys. Rev.* B **35** 8154
White S M and Sham L J 1981 *Phys. Rev. Lett.* **47** 879